# Mechanical Tuning of Fluorescence Lifetime and Bandgap in an Elastically Flexible Molecular Semiconductor Crystal

Arif Hassan Dar[#],[a] Atiqur Rahman[#],[a] Srijan Mondal,[a] Argha Barman,[a] Monika Gupta,[a] Pramit K. Chowdhury,[a] and Sajesh P. Thomas*[a]

(Dedication….)

[a] Department of Chemistry, Indian Institute of Technology Delhi, New Delhi, 110016, India
E-mail: sajesh@iitd.ac.in

# These authors contributed equally

Supporting information for this article is given via a link at the end of the document.

**Abstract:** Despite having superior transport properties, lack of mechanical flexibility is a major drawback of crystalline molecular semiconductors as compared to their polymer analogues. Here we report single crystals of an organic semiconductor that are not only flexible but exhibit systematic tuning of bandgaps, fluorescence lifetime, and emission wavelengths upon elastically bending. Spatially resolved fluorescence lifetime imaging and confocal fluorescence microscopy reveal systematic trends in the lifetime decay across the bent crystal region along with shifts in the emission wavelength. From the outer arc to the inner arc of the bent crystal, a significant decrease in the lifetime of ~1.9 ns was observed, with a gradual bathochromic shift of ~10 nm in the emission wavelength. For the crystal having a bandgap of 2.73 eV, the directional stress arising from bending leads to molecular reorientation effects and variations in the extent of intermolecular interactions– which are correlated to the lowering of bandgap and the evolution of the projected density of states. The systematic changes in the interactions quantified using electron density topological analysis in the compressed inner arc and elongated outer arc region are correlated to the non-radiative decay processes, thus rationalizing the tuning of fluorescence lifetime. Such mechanical tuning of band gaps and photophysical properties may pave the way to innovative technologies in the micro-fabrication of flexible organic functional materials such as semiconductors and organic light-emitting diodes.

## Introduction

Among the two major classes of materials used in organic electronics, crystalline molecular semiconductor materials have several advantages over polymer materials. Molecular crystals offer higher charge carrier mobility, better interface compatibility, and structural control at the molecular and intermolecular level which make them suitable for single-crystal device fabrication, and for applications in solar cells, organic light-emitting diodes,[1,2] and organic field-effect transistors.[3,4] However, a major disadvantage of crystalline semiconductor materials, in general, is their lack of mechanical flexibility (ability to deform with applied stress- while maintaining the integrity of the crystal structure) which poses challenges in device fabrication. This challenge can be addressed within the fast-growing research field of dynamic molecular crystals. Flexible molecular crystals[5–9] with many interesting applications in the field of optoelectronics,[10] mechanical actuating devices,[11,12] waveguides,[13,14] sensors,[15] and wearable devices[16] have been reported recently. As high crystallinity implies an absence of impurity and structural imperfections (and better carrier mobility), these materials offer better device performance than devices made of amorphous materials.[4] Recent reports of higher field-effect mobility and increased conductivity in flexible semiconducting molecular crystals point to the prospects of utilizing flexible crystals in organic electronics.[17,18] Modulation in intermolecular interactions and the associated electron density features that lead to the variation in the photophysical properties of molecular crystals upon bending remain largely underexplored. In this direction, various micro-focused studies including μ-XRD mapping,[19–21] μ-Raman mapping,[22–25] and photoluminescence (PL) measurements [26–28] across the bent crystal region have been reported. A structural model of the bent crystal region with a lattice compression in the inner arc and expansion in the outer arc facilitated by molecular re-orientation has been accepted widely – as evidenced by the μ-XRD mapping study by Clegg et al.[19,21] Recently, we estimated a local stress difference of ~2 GPa experienced by the molecules across the elastically bent region of a lipidated molecular crystal.[29] These structural changes and internal stress upon bending can translate into variations in the physical properties of molecular crystals in the bent crystal region.[30,31] Here, we report for the first time, a systematic variation in the fluorescence lifetime upon crystal bending- along with μ-PL mapping that reveals a gradual bathochromic shift in emission wavelengths from the outer arc to the inner arc of the bent crystal of **1.** We have employed confocal fluorescence microscopy (CFM) along with fluorescence lifetime imaging (FLIM) across the bent crystal region, to probe the tuning of emission wavelengths and fluorescence lifetime – two key properties of an optoelectronic material- in the single crystals of acenaphthoquinone (compound **1**; Figure 1a) upon elastically bending. Lifetime is a crucial property of semiconductors closely linked to the recombination of excitons and carrier dynamics in the materials. To our knowledge, lifetime variation across a bent molecular crystal is not been observed before.[24] Although the change in bandgaps with the extent of bending in coronene crystals has been recently reported by Gong et al,[18] the bandgap variation across the bent region of flexible molecular crystals remains underexplored. Here we have explored this aspect using uniaxial pressure simulation along with quantum periodic calculations of the band structure. Along with bandgaps, we have investigated the possible changes in the projected density of states due to the structural perturbations upon bending and correlated the changes in intermolecular interactions with the observed shifts in emission wavelengths and tuning in the lifetime.

## Results and Discussions

**Elastic bending and its correlation with crystal packing.** Single crystals of **1** were crystallized in the $P2_12_12_1$ space group with cell parameters $a$ = 3.7723 (3) Å, $b$= 7.8283 (7) Å, $c$ = 26.756 (2) Å, Z = 4, and Z' = 1. π···π stacking along [100] direction is the dominant intermolecular interaction that dictates the crystal growth, leading to

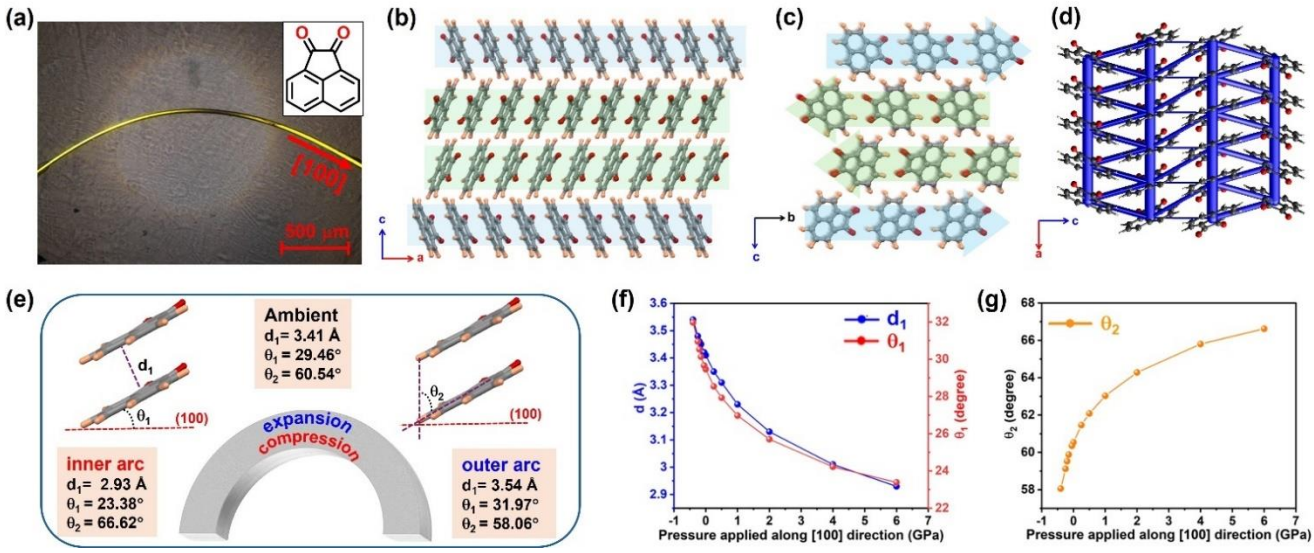


**Figure 1.** (a) Molecular structure of compound **1**, and the crystal of **1** in the elastically bent state. (b) Crystal packing diagram viewed down *b*-axis showing π···π stacking along [100] direction. (c) Crystal packing is viewed down the *a*-axis. (d) Interaction topology ('energy frameworks') viewed down the *b*-axis. (e) Molecular orientational changes along with lattice compression and elongation upon uniaxial pressure applied along needle direction. (f,g) Variation of intermolecular π···π stacking distance ($d_1$) and angles ($\theta_1$ and $\theta_2$) describing the molecular orientations.

the acicular morphology of the crystals with [100] as the acicular crystal growth direction. Upon applying mechanical force, these needle-shaped crystals were found to be elastically bending with the bending direction as [100] and (001) face as the bending face. The observed bending in crystals of **1** can be rationalized based on the intermolecular interaction topology (energy frameworks) showing the strongest supramolecular column along [100] – similar to the several examples reported earlier (Figure 1d).[32,33] Higher dispersion energy contribution (-56.0 kJ/mol) along the *a*-axis to total pairwise interaction energy (-28.8 kJ/mol) corresponding to π···π stacking supports the crystal growth along the [100] direction (Figure 1b,d and Figure S5, dimer 1). The mean molecular planes forming the π···π stacks are oriented with an angle of 29.46˚ to (100) plane and with a mean inter-molecular distance of 3.41 Å (See $\theta_1$ and $d_1$ in Figure 1e). The molecular orientational changes upon bending can be described as the variations in $\theta_1$. The packing along nearly orthogonal directions is mainly stabilized because of C–H···O Å and C–H···π interactions (with strengths -19.1 kJ/mol, -16.1 kJ/mol respectively; see Figure S5). Especially, the C–H···O interaction motif binds the stacked molecular columns -possibly preventing inter-stack slipping upon bending as it has a strong electrostatic component arising from the head-to-tail orientation of the molecular dipoles in this dimer motif (Figure 1c and Figure 6e-f).

**Probing the structural flexibility: Thermal expansion behaviour, high-pressure simulations, and elastic tensor analysis.** To understand the effects of anisotropy in crystal packing and interaction strengths, the thermal expansion behaviour of **1** was studied by variable temperature single-crystal XRD (Figure 2a). The highest thermal expansion was observed along [100] direction (Figure 2a,b). This is unusual considering that the strongest interactions in the topology are along the [100] direction. A possible origin of this anomalous thermal expansion behaviour could be the dominant contribution of the dispersion and repulsion components (-56 and 30.6 kJ/mol respectively) to total pairwise interaction energy (-28.8 kJ/mol) (Figures S4, S6). [001] direction shows an expansion lower than that along [100], while [010] shows negligible expansion. These results correlate with the trends in compressibility observed from hydrostatic pressure simulations (Figure 2c), in which deformation with pressure was found to be highest along [100] direction. Further, to mimic the directional stress experienced by the crystal upon elastic bending, we performed uniaxial pressure simulations by applying variable pressure along [100] direction (Figure 2d). The positive values of the uniaxial pressure simulate the structural changes in the compressed inner arc region, while the negative values model the tensile stress and elongation along [100] in the outer arc region of a bent crystal. The major structural change in π···π stacked crystal structures upon bending is in the intermolecular orientations with compression in the inner arc and elongation in the outer arc region - as demonstrated by Clegg et al in the case of Cu(acac)$_2$.[19] We observed a decrease in angle $\theta_1$ from 29.46˚ to 25.70˚ upon uniaxial compression (2 GPa) along [100] direction (Figure 1f), whereas an increase up to 31.97˚ in case of expansion (-0.40 GPa).

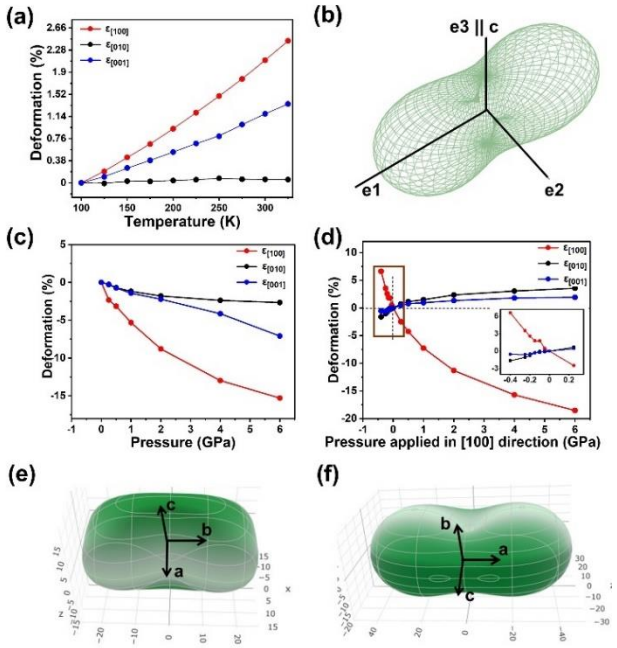


**Figure 2:** (a) Deformation in the unit cell parameters of **1** with temperature, (b) TEV plot showing maximum expansion along *a*-axis. (c,d) Percentage deformation in the unit cell parameters with simulated hydrostatic and uniaxial pressure along [100] directions. (e,f) Spatial distribution of Young's moduli and linear compressibility plot of **1**.

This clearly indicates the molecular orientational changes upon bending. In addition to intermolecular orientational changes, we observe a decrease in the π···π planar distance (from 3.41 Å in the ambient pressure to 3.13 Å at 2 GPa) under compression, and an increase (3.41 Å to 3.54 Å) in case of expansion (-0.40 GPa – mimicking the tensile stress).

Further, elastic tensor analysis of **1** was performed using the S-HF-3c method[34,35] with CRYSTAL17[36] and the mechanical properties were visualized using the ELATE tool.[37] The spatial distribution of Young's modulus (*E*) reveals the following trend as shown in Figure 2e: $E_{[010]} > E_{[001]} > E_{[100]}$. Among the three orthogonal directions of the crystal, the maximum value of *E* was found to be along the *b*-direction (25.0 GPa) and the minimum along [100] direction (10.6 GPa) leading to an anisotropy of ~ 2.5 in Young's moduli (Figure S8). This trend correlates with the maximum linear compressibility (K) observed along the [100] direction (48.0 $TPa^{-1}$), a much lower value along the [001] direction (29.9 $TPa^{-1}$), and the lowest along [010] direction (7.2 $TPa^{-1}$) respectively (Figure 2f). These results from the computed elastic constants agree with the experimentally observed thermal expansion behaviour.

**Effect of bending on bandgaps and the electronic band structure.** The structural changes such as the molecular re-orientational effects and the gradual tuning of π···π stacking observed in the bent crystal regions prompted us to investigate the associated changes in the electronic bandgaps in this semiconductor crystal. UV-Vis diffuse reflectance spectra of the crystalline solid sample of **1** indicated a band gap of 2.73 eV (Figure 3e). Further, quantum periodic calculations of the band structure of **1** performed at different hydrostatic pressure points (from ambient to 6 GPa) show that $E_{gap}$ values systematically decrease with the pressure- as expected in most materials (Figure 3f). Intriguingly, when uniaxial pressure is applied along [100] to simulate the changes in the bent crystal region a counterintuitive trend in the bandgap is observed. For the uniaxial pressure range of 0 to 2 GPa (mimicking the inner arc region), a systematic increase in $E_{gap}$ values followed by a decrease from the 2-6 GPa range was observed (Figure 3g). Whereas from 0 to -0.40 GPa (mimicking the tensile stress upon elongation in the outer arc region) the $E_{gap}$ values show a slight decrease from 2.73 eV to 2.70 eV (Figure 3g). The projected density of state indicates that the states corresponding to C atoms tend to dominate the valence band edge in the band structure of 1 with compression in the inner arc – as opposed to the ambient structure in which states associated with O atoms form the valence band edge (Figure 3a-c). For a molecular-level understanding of these changes in the band structure, we calculated the HOMO-LUMO energy gaps and dipole moments corresponding to the three major supramolecular dimers and their changes with the applied uniaxial pressure (Figure 3d,h and Table S9). A systematic decrease in the HOMO-LUMO gap and dipole moment for the π···π stacking dimer 1 was notable upon uniaxial compression along the *a*-axis. However, the HOMO-LUMO gap corresponding to the C-H···O hydrogen bonded dimer 2, shows only slight variation with compression/elongation (Figure 3d). Since dimer 3 shows an opposite trend in the HOMO-LUMO gap to that in dimer 1, a combination of these effects might explain the variation in bandgap as found in Figure 3g. Our results are in line with the 7-fold enhancement in the conductivity of coronene crystals upon bending recently reported by Gong et al, which was associated with a decrease in energy difference between LUMO and Fermi level ($E_F$) with an increase in bending degree (smaller radius of curvature) by the analysis of valence band spectra using X-ray photoelectron spectroscopy (XPS).[18]

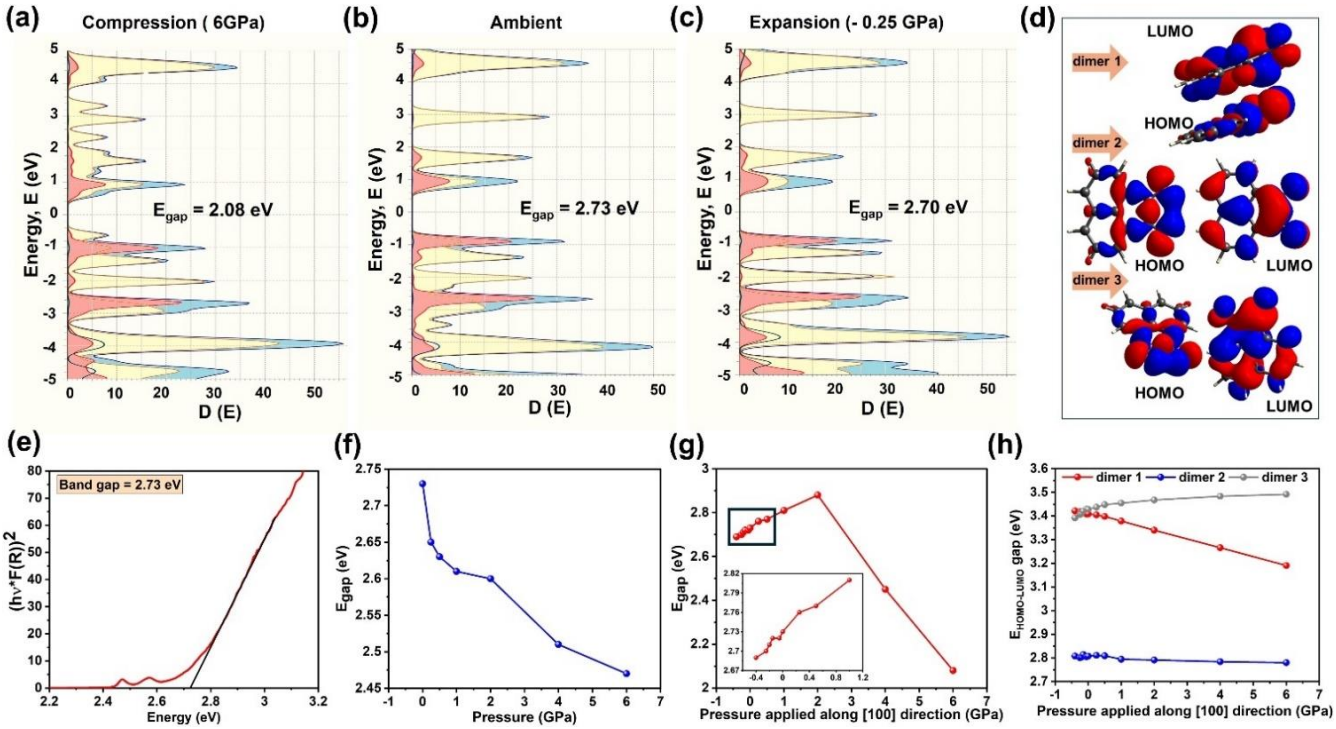


**Figure 3:** (a-c) Electronic band structure of **1** calculated at different geometries obtained after pressure applied along [100] direction (colour code: total – blue, Carbon – yellow, Oxygen – red, and Hydrogen - black line. (d) HOMO-LUMO plotted for dimer 1, dimer 2 and dimer 3. (e) Tauc plot for band gap calculation. (f) Band gap calculated for optimized geometries after applying hydrostatic pressure, (g) uniaxial pressure along [100] direction. (h) Variation in the HOMO-LUMO gap with uniaxial pressure along [100].

**Tuning of fluorescence emission wavelengths and lifetime across the bent crystal region.**

Further, we set out to investigate the effects of structural changes and the evolution of band structure on photophysical properties such as fluorescence emission wavelength and lifetime. To our knowledge, there is no report of changes in fluorescence lifetime across bent regions of molecular crystals. A few earlier studies on bent molecular crystals have probed the changes in PL emission wavelengths and intensities in the bent vs straight crystal regions (Table 1). Three of these reported studies investigated spatially resolved spectral changes from the inner arc to outer arc regions of the bent crystals- with contradictory trends. This implies that the tuning of photophysical properties can be highly structure-dependent, and the trends in emission properties could vary with respect to the perturbations in the supramolecular environments in crystals upon bending. Since these properties are crucial features of flexible semiconductors and optoelectronic materials, we employed spatially resolved techniques of FLIM and CFM on the bent crystal of **1.**

For the spatially resolved CFM studies, elastically bent crystals of **1** were fixed on a glass slide and excited using a pulsed white light laser (WLL) with an excitation wavelength of 532 nm (Figure 4b). The lateral resolution of ~300 nm used in the CFM ensured a high spatial separation of the points imaged. A systematic bathochromic shift in emission spectra from 585.3 nm to 595.1 nm was observed from the outer arc to the inner arc measured at 7 different points within a focus area of 3.5 × 3.3 $\mu m^2$ in the bent crystal region of **1** (of thickness ~ 26.4 μm, Figure 4c-e). As a control experiment, we performed a similar PL spectral mapping across an unbent crystal of **1** with no deformation or strain. No significant shift in emission spectra (590.5 nm) was observed in the case of this straight crystal (thickness ~ 38 μm) measured at 7 different points each with an area of 4.5 × 4.0 $\mu m^2$ (Figure 4a,f). The standard deviation and standard error on the emission wavelengths for straight crystal were estimated to be 1.26 nm and 0.47 nm respectively- further validating the reliability of the bathochromic shifts observed across the bent region (See Table S10 for details).

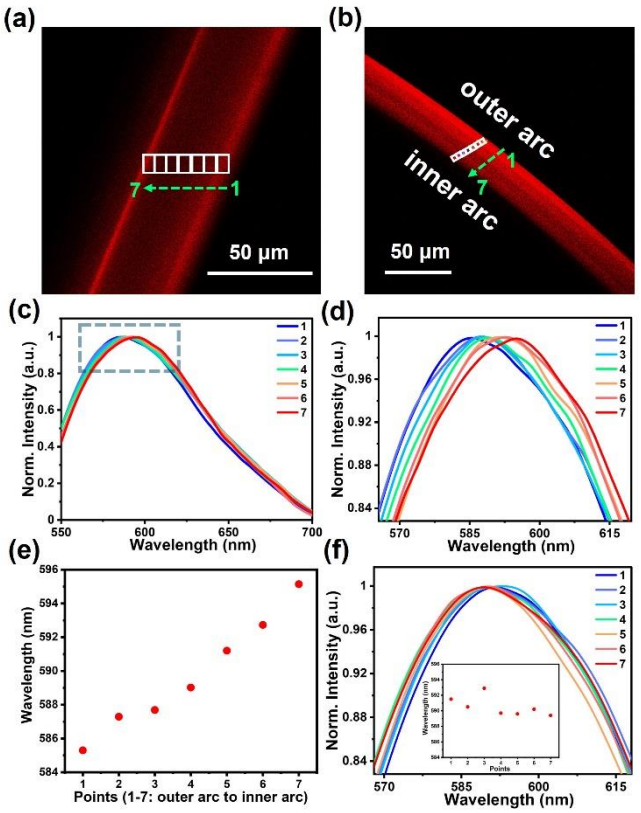


**Figure 4.** (a,b) Image of straight and bent crystal of the probed crystal region. (c) Emission spectra of bent crystal of **1** (1 to 7: outer arc to inner arc) over the wavelength range of 550 – 700 nm, (d) A part of the emission spectra as shown by the box in (c) have been zoomed in to highlight the systematic redshifts in the emission maxima. (e) Redshifts in the emission maxima from the outer arc to the inner arc of the bent crystal of **1**. (f) Emission spectra measured on seven different points on the unbent crystal across the thickness showing no significant shifts.

**Table1.** Spatially resolved photoluminescence studies reported on flexible molecular crystals and the structure-based rationalization/explanation for the observed trends.

| S.No. | Compound | Flexibility | Mapping | Shifts | | Rationalization |
|---|---|---|---|---|---|---|
| | | | | Inner arc | Outer arc | |
| 1 | 1,4-Bis[2-(4-methylthienyl)]-2,3,5,6-tetrafluorobenzene | elastic[26] | no | blue shift after bending | | slipping of the π···π planes causes inhibition of the efficient energy transfer between the molecules |
| 2 | Flufenamic acid form III | plastic[38] | no | blue shift after bending | | looser crystal packing and weakening of aromatic interactions |
| 3 | 1,4-bisthienyl-2,3,5,6-tetrafluorobenzene | elastic[39] | yes | no significant shift | blue shift (2 nm) | sliding of the molecular plane between π···π interactions |
| 4 | TPABA | multi-facet elastic[40] | (002) face | red shift (26 nm) | blue shift (4 nm) | variation in π···π interaction distance and number of such interactions on different crystal surface |
| | | | (200) face | blue shift (2 nm) | red shift (3 nm) | |
| 5 | GFPC | plastic[28] | | increasing the emission intensity | | restriction of intramolecular motions |
| 6 | 9,10-dibromoanthracene | elastic[27] | yes | blue shift (3 nm) | red shift (6 nm) | H-aggregation and J-aggregation upon bending |
| 7 | DBBTPAT | elastic[41] | elastically bent | red shift at bent region (20 nm) | | conformational change |
| | | | naturally bent | red shift at bent region (16 nm) | | |
| 8 | MMIAB | elastic[42] | no | blue shift upon stretching | | increase in π···π planar distance |
| 9 | fluorenol-carbazole | elastic[24] | yes | fluorescence intensity decreases | | enhanced non-radiative transition |
| | | | | no variation in lifetime* | | |
| 10 | Compound 1 (this work) | elastic | | red shift (5 nm) | blue shift (5 nm) | See the discussion in the following section |

Further to study the variation in fluorescence lifetime in the bent crystal region, we carried out FLIM measurements on the bent single crystal of **1**. The crystal was excited using a pulsed diode laser of wavelength 532 nm and fluorescence decays were collected at 6 different points across the thickness (~ 41 μm) of the bent crystal. The obtained decays were fitted to a sum of three exponential components ($\tau_1$,$\tau_2$, and $\tau_3$). A systematic decrease in the average fluorescence lifetime ($\tau_{avg}$) was observed from 2.46 ns to 0.54 ns from an expanded outer arc to the compressed inner arc region of bent crystal, these $\tau$ being measured at 6 different points across the thickness (~ 41 μm) of the bent crystal (Figure 5d-f). This is a significant change in lifetime in comparison to the reported values of lifetime variation with a change in supramolecular environment or pressure.[43,44] The only previous study on the lifetime for a bent crystal of elastically flexible fluorenol-carbazole crystal by Wei *et al* reported no notable variation in the lifetime in the bent region.[24] In the case of **1**, the gradual tuning in lifetime can be visualized as the clear color gradient from red to light blue – indicating the highest value of lifetime in the outer arc region to the lowest lifetime observed in the inner arc region of the bent crystal (Figure 5d). This trend is clearly in contrast with the FLIM maps of the straight crystal on which only a single color can be seen, with no significant variation in a lifetime (Figure 5a). This is in agreement with the CFM measurements on the straight crystal, in which no shift in $\lambda_{max}$ was observed (Figure 4f). The standard deviation and standard error in lifetime calculated from the lifetime data for straight crystal were found to be 0.07 ns and 0.03 ns respectively (Table S12) – based on the data collected on 5 different points of the straight crystal across a thickness of ~39 μm (Figure 5a-c). The average lifetime of the unperturbed straight crystal is found to be 1.77 ns. This value is quite close to the lifetime observed at the middle point of the bent crystal - indicating the systematic nature of the lifetime tuning induced by mechanical bending. Repeated measurements on the bent crystals of 1 confirmed the reproducibility in the trends of wavelength shifts and lifetime variation across the bent region (Figure S12, Table S10, Figure S13, and Table S11).

**Rationalization of the shifts in emission wavelengths and lifetime based on the bending model.** Shifts in the PL emission with varying pressure are a commonly observed phenomenon in nanoparticles,[45] quantum dots[46,47] and molecular systems.[48–50] High-pressure photoluminescence studies on molecular crystals also have revealed a similar trend of red shifts in emission wavelengths with an increase in pressure.[51,52] In general, such shifts in $\lambda_{em}$ and $\tau_{avg}$ are rationalized based on the following arguments: (i) variations in J or H-aggregate character of the supramolecular assemblies, (ii) changes in the extents of intermolecular separations and orbital interactions. As it is understood from various proposed bending models[53,54] and experimentally mapped μ–focus studies,[19,21] the lattice of the bent crystal gets compressed in the inner arc and expanded in the outer arc. Here, our uniaxial-pressure studies show an increase in the slip angle ($\theta_2$) in the π···π stacked dimer 1 from 60.54° to 64.28° upon compression (Figure 1g), leading to a slight enhancement in H-aggregate character in the compressed region (Table S8). However, this structural change would not be sufficient to rationalize the observed red shift in the inner arc – as it is contrary to the hypsochromic shifts associated with the H-aggregate character. Similarly, dimer 2 shows an intermolecular orientation with a perfect head-to-tail alignment of molecular dipole moment vectors as in a J-aggregate (Figure 6d-f). The electrostatic nature of this C–H···O interaction motif is also evident in the electron deformation density plot derived from X-ray quantum crystallographic Hirshfeld Atom Refinement (Figure 6e).[55] While the molecular dipole moment for the isolated molecule of 1 was found to be 6.3 D, that for the crystal determined from X-ray quantum crystallography (which incorporates crystal field effects) was found to be 8.7 D. The changes in their orientation upon compression/elongation are found to be small from our analysis (Table S8). Nevertheless, given that the crystal packing is non-centrosymmetric, the effect of such subtle dipole-dipole orientational changes on the photophysical properties is yet to be understood.

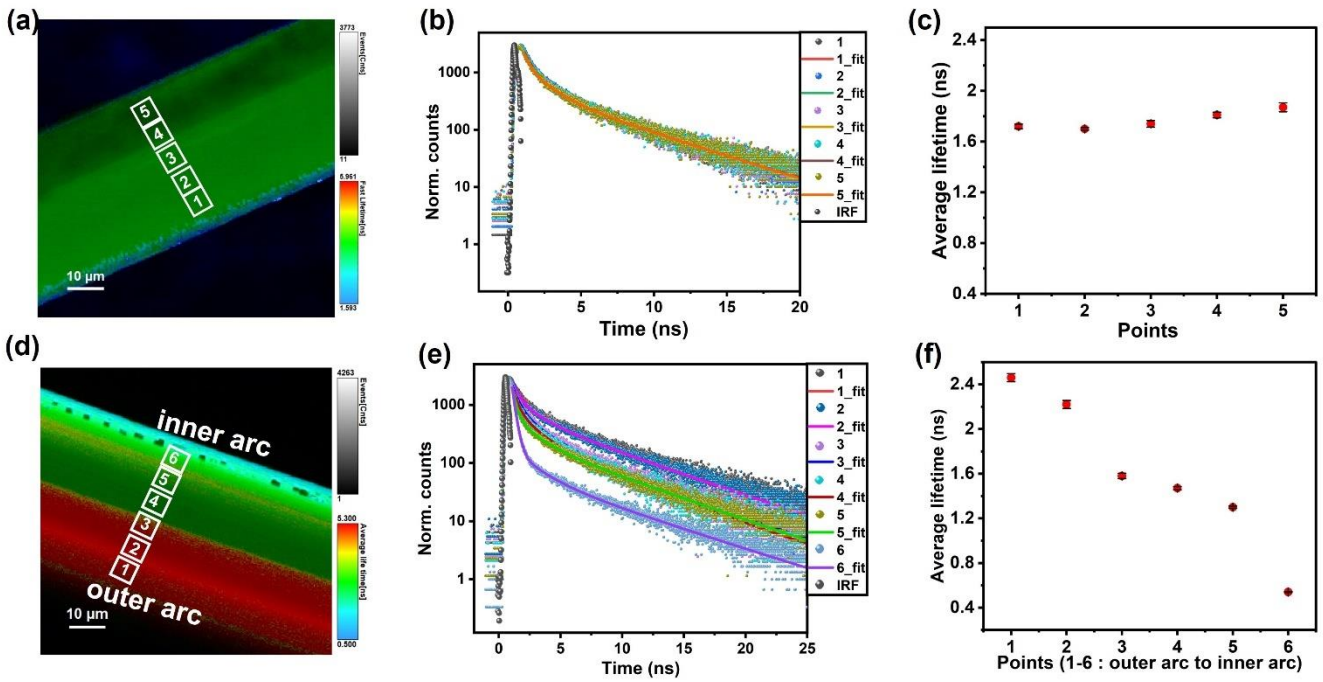


**Figure 5:** (a,d) Fluorescence lifetime Image of straight and bent crystal of **1**. (b,e) Lifetime decay plot (log scale) at different regions of the straight and bent crystal of **1** respectively. (c) Average lifetime at different points on the straight crystal, and (f) bent crystal (outer arc to inner arc).

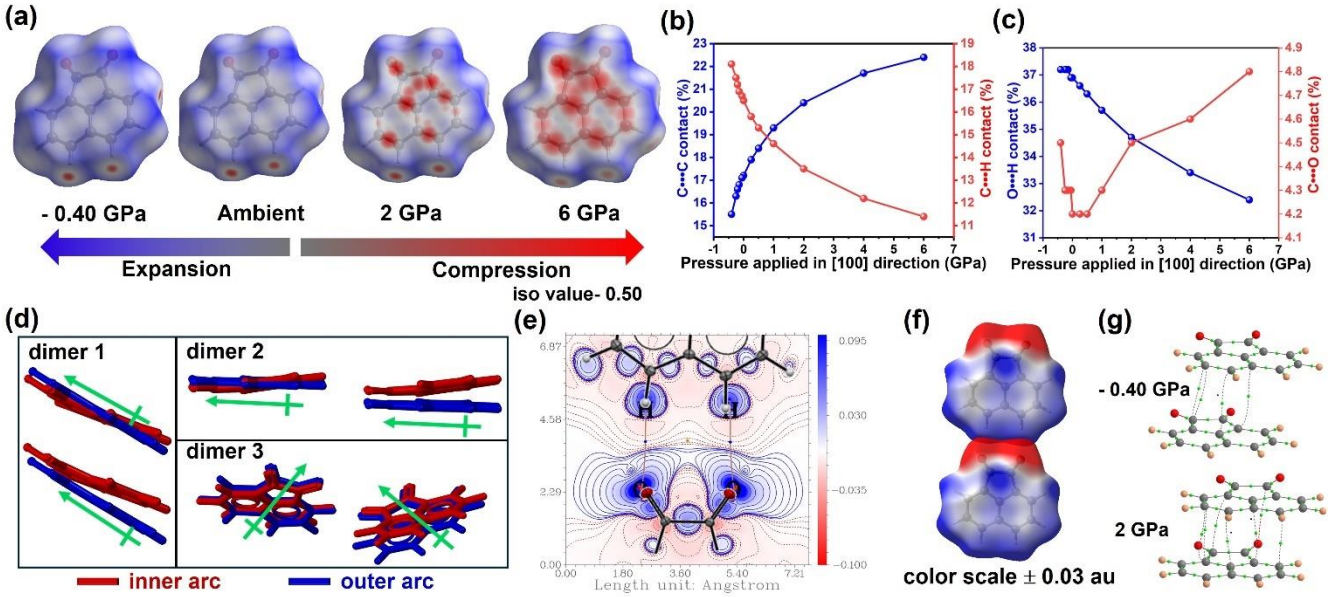


**Figure 6:** (a) Variations in intermolecular interactions with expansion and compression along [100] direction, manifested on Hirshfeld surface of 1. (b,c) Variation in contact percentage with uniaxial pressure. (d) Orientation of dipoles in the three dominant molecular pairs, (e) X-ray quantum crystallography derived electron deformation density plot showing the strong electrostatic nature of the C–H···O interaction motif in dimer 2. (f) Electrostatic potential mapped on the Hirshfeld surfaces revealing the J-aggregate nature of dimer 2, (g) Molecular graphs showing an increase in a number of bond paths from expanded structure (-0.40 GPa) to compressed structure (2 GPa) in dimer 1.

Notably, the uniaxial compression along [100] direction results in a systematic decrease in the interplanar distance, $d_1$ (π···π interaction distance) from 3.41 Å to 3.13 Å (Table S8). This trend is further evident from the systematic changes in the percentages of intermolecular atom…atom contacts quantified using Hirshfeld fingerprint plots. The crystal structures corresponding to the expanded outer arc to the compressed inner arc show a systematic increase in the C···C contact percentage values, while those of C···H and H···O contacts show an opposite trend (Figure 6a-c). This points to an increase in the degree of π…π overlapping and a decrease in the interplanar distance in the inner arc region. This trend is further quantified by an electron density topological analysis on dimer 1, which reveals the number of C···C bond paths corresponding to π···π interaction show an increase with compression and a decrease with elongation. Moreover, a systematic increase in the values of topological parameters such as electron density (ρ) and its Laplacian ($\nabla^2\rho$) for π···π interaction in dimer **1**, and the associated values of potential energy density, kinetic energy density estimated at the bond critical points (bcp) also clearly shows increments due to the enhanced intermolecular interactions with compression (Figure 6g, Table S3). Thus the decrease in interaction distances, and increase in intermolecular atom…atom contacts in the inner arc region upon bending as evident from Figure 6a can imply enhanced non-radiative decay processes/ self-quenching and thereby explain the observed decrease in lifetime.[43] Moreover, the increased electron density values at the bcps corresponding to π···π interactions can be correlated to the decreased HOMO-LUMO energy gap in the inner arc region, which in turn leads to the bathochromic shifts.

## Conclusions

In summary, we have demonstrated elastic bending and the associated changes in electronic and photophysical properties in semiconductor single crystals of **1**. Our study provides the first example of the tuning of fluorescence lifetime achieved by the mechanical bending of crystals. The counterintuitive trend of bandgap lowering on both the inner and outer arc of the bent crystal, as revealed in this study, provides insights into the examples of enhanced electronic conductivity and carrier mobility upon crystal bending, which were reported recently.[17,18] The significantly distinct trends in bandgap with hydrostatic pressure and the uniaxial pressure upon bending reveal that there is more to understand about the structural dynamics upon bending, beyond lattice compression and shortening of interactions. Moreover, we have observed the systematic tuning of emission wavelengths (5 nm red-shifted in the inner arc and 5 nm blue-shifted in the outer arc as compared to an unbent crystal). We have correlated the tuning of the properties with the changes in the micro-environment and the extent of various intermolecular interactions in the inner and outer arc regions of the bent crystals – with a quantitative analysis of the electron density topological features. These results point to the prospects for mechanical control of properties and new strategies in fabricating semiconductors/ optoelectronic devices based on flexible molecular materials.

## Acknowledgements

S.P.T. thanks DST-SERB for a Starting Research Grant (SRG/2022/001852) and IIT Delhi for a Seed grant. S.P.T. and A.R. thank DST: SR/FST/CSII-07/2014 and the Institute of Eminence (IOE) grant from the University Grants Commission (UGC-Ministry of Human Resource and Development, India) for funding the single-crystal diffractometers at the Department of Chemistry, IIT Delhi. A.H.D. thank DST-SERB for NPDF funding (PDF/2022/000567) and A.R. thanks UGC for the Junior Research Fellowship and UQIDAR for a research fellowship. We thank the SATHI Foundation IIT Delhi for time-resolved fluorescence measurements.

**Keywords** Flexible crystals, photophysical properties, organic semiconductor, fluorescence lifetime

## References

[1] L. Gu, H. Shi, L. Bian, M. Gu, K. Ling, X. Wang, H. Ma, S. Cai, W. Ning, L. Fu, H. Wang, S. Wang, Y. Gao, W. Yao, F. Huo, Y. Tao, Z.

An, X. Liu, W. Huang, *Nat. Photonics* **2019**, *13*, 406–411.
[2] W. Ye, H. Ma, H. Shi, H. Wang, A. Lv, L. Bian, M. Zhang, C. Ma, K. Ling, M. Gu, Y. Mao, X. Yao, C. Gao, K. Shen, W. Jia, J. Zhi, S. Cai, Z. Song, J. Li, Y. Zhang, S. Lu, K. Liu, C. Dong, Q. Wang, Y. Zhou, W. Yao, Y. Zhang, H. Zhang, Z. Zhang, X. Hang, Z. An, X. Liu, W. Huang, *Nat. Mater.* **2021**, *20*, 1539–1544.
[3] V. Coropceanu, J. Cornil, D. A. da Silva Filho, Y. Olivier, R. Silbey, J.-L. Brédas, *Chem. Rev.* **2007**, *107*, 926–952.
[4] A. L. Briseno, R. J. Tseng, M.-M. Ling, E. H. L. Falcao, Y. Yang, F. Wudl, Z. Bao, *Adv. Mater.* **2006**, *18*, 2320–2324.
[5] A. J. Thompson, A. I. Chamorro Orué, A. J. Nair, J. R. Price, J. McMurtrie, J. K. Clegg, *Chem. Soc. Rev.* **2021**, *50*, 11725–11740.
[6] E. Ahmed, D. P. Karothu, P. Naumov, *Angew. Chemie Int. Ed.* **2018**, *57*, 8837–8846.
[7] P. Naumov, S. Chizhik, M. K. Panda, N. K. Nath, E. Boldyreva, *Chem. Rev.* **2015**, *115*, 12440–12490.
[8] C. Wei, L. Li, Y. Zheng, L. Wang, J. Ma, M. Xu, J. Lin, L. Xie, P. Naumov, X. Ding, Q. Feng, W. Huang, *Chem. Soc. Rev.* **2024**.
[9] W. M. Awad, D. W. Davies, D. Kitagawa, J. Mahmoud Halabi, M. B. Al-Handawi, I. Tahir, F. Tong, G. Campillo-Alvarado, A. G. Shtukenberg, T. Alkhidir, Y. Hagiwara, M. Almehairbi, L. Lan, S. Hasebe, D. P. Karothu, S. Mohamed, H. Koshima, S. Kobatake, Y. Diao, R. Chandrasekar, H. Zhang, C. C. Sun, C. Bardeen, R. O. Al-Kaysi, B. Kahr, P. Naumov, *Chem. Soc. Rev.* **2023**, *52*, 3098–3169.
[10] S. Hayashi, T. Koizumi, N. Kamiya, *Cryst. Growth Des.* **2017**, *17*, 6158–6162.
[11] J. M. Halabi, E. Ahmed, S. Sofela, P. Naumov, *Proc. Natl. Acad. Sci. U. S. A.* **2021**, *118*.
[12] S. Chizhik, A. Sidelnikov, B. Zakharov, P. Naumov, E. Boldyreva, *Chem. Sci.* **2018**, *9*, 2319–2335.
[13] M. Annadhasan, A. R. Agrawal, S. Bhunia, V. V. Pradeep, S. S. Zade, C. M. Reddy, R. Chandrasekar, *Angew. Chemie Int. Ed.* **2020**, *59*, 13852–13858.
[14] S. Hayashi, S. Yamamoto, D. Takeuchi, Y. Ie, K. Takagi, *Angew. Chemie Int. Ed.* **2018**, *57*, 17002–17008.
[15] L. Lan, X. Yang, B. Tang, X. Yu, X. Liu, L. Li, P. Naumov, H. Zhang, *Angew. Chemie Int. Ed.* **2022**, *61*, e202200196.
[16] X. Yang, L. Lan, L. Li, X. Liu, P. Naumov, H. Zhang, *Nat. Commun.* **2022**, *13*, 2322.
[17] R. Samanta, S. Das, S. Mondal, T. Alkhidir, S. Mohamed, S. P. Senanayak, C. M. Reddy, *Chem. Sci.* **2022**, *14*, 1363–1371.
[18] Y. Chen, Z. Chang, J. Zhang, J. Gong, *Angew. Chemie Int. Ed.* **2021**, *60*, 22424–22431.
[19] A. Worthy, A. Grosjean, M. C. Pfrunder, Y. Xu, C. Yan, G. Edwards, J. K. Clegg, J. C. McMurtrie, *Nat. Chem.* **2018**, *10*, 65–69.
[20] S. P. Thomas, A. Worthy, E. Z. Eikeland, A. J. Thompson, A. Grosjean, K. Tolborg, L. Krause, K. Sugimoto, M. A. Spackman, J. C. McMurtrie, J. K. Clegg, B. B. Iversen, *Chem. Mater.* **2023**, *35*, 2495–2502.
[21] B. Bhattacharya, A. A. L. Michalchuk, D. Silbernagl, N. Yasuda, T. Feiler, H. Sturm, F. Emmerling, *Chem. Sci.* **2023**, *14*, 3441–3450.
[22] M. K. Panda, S. Ghosh, N. Yasuda, T. Moriwaki, G. D. Mukherjee, C. M. Reddy, P. Naumov, *Nat. Chem.* **2015**, *7*, 65–72.
[23] K. Wang, M. K. Mishra, C. C. Sun, *Chem. Mater.* **2019**, *31*, 1794–1799.
[24] C. Wei, L. Bai, C. Wei, L. Bai, X. An, M. Xu, W. Liu, W. Zhang, M. Singh, *Chem.* **2022**, *8*, 1427–1441.
[25] M. K. Mishra, K. Mishra, S. A. Syed Asif, P. Manimunda, *Chem. Commun.* **2017**, *53*, 13035–13038.
[26] S. Hayashi, T. Koizumi, *Angew. Chemie Int. Ed.* **2016**, *55*, 2701–2704.
[27] S. Hayashi, F. Ishiwari, T. Fukushima, S. Mikage, Y. Imamura, M. Tashiro, M. Katouda, *Angew. Chemie Int. Ed.* **2020**, *59*, 16195–16201.
[28] B. Bhattacharya, D. Roy, S. Dey, A. Puthuvakkal, S. Bhunia, S. Mondal, R. Chowdhury, M. Bhattacharya, M. Mandal, K. Manoj, P. K. Mandal, C. M. Reddy, *Angew. Chemie Int. Ed.* **2020**, *59*, 19878–19883.
[29] A. Rahman, S. Mondal, M. Modak, A. Singh, H. Singh, N. S. Thayat, K. Clegg, H. K. Poswal, V. Haridas, S. P. Thomas, *ChemRxiv* **2024**, *1*, 0–6.
[30] E. Ahmed, D. P. Karothu, L. Pejov, P. Commins, Q. Hu, P. Naumov, *J. Am. Chem. Soc.* **2020**, *142*, 11219–11231.
[31] E. P. Kenny, A. C. Jacko, B. J. Powell, *Angew. Chemie Int. Ed.* **2019**, *58*, 15082–15088.
[32] M. J. Turner, S. P. Thomas, M. W. Shi, D. Jayatilaka, M. A. Spackman, *Chem. Commun.* **2015**, *51*, 3735–3738.
[33] S. P. Thomas, M. W. Shi, G. A. Koutsantonis, D. Jayatilaka, A. J. Edwards, M. A. Spackman, *Angew. Chemie Int. Ed.* **2017**, *56*, 8468–8472.
[34] R. Sure, S. Grimme, *J. Comput. Chem.* **2013**, *34*, 1672–1685.
[35] P. R. Spackman, A. Grosjean, S. P. Thomas, D. P. Karothu, P. Naumov, M. A. Spackman, *Angew. Chemie - Int. Ed.* **2022**, *61*.
[36] R. Dovesi, A. Erba, R. Orlando, C. M. Zicovich-Wilson, B. Civalleri, L. Maschio, M. Rérat, S. Casassa, J. Baima, S. Salustro, B. Kirtman, *Wiley Interdiscip. Rev. Comput. Mol. Sci.* **2018**, *8*, 1–36.
[37] R. Gaillac, P. Pullumbi, F.-X. Coudert, *J. Phys. Condens. Matter* **2016**, *28*, 275201.
[38] Y. Liu, P. Yang, K. Zhang, J. Xu, S. Wu, J. Gong, *Cryst. Growth Des.* **2022**, *22*, 1312–1318.
[39] S. Hayashi, *CrystEngComm* **2021**, *23*, 5763–5767.
[40] J. Peng, C. Han, S. Li, X. Cao, J. Bai, J. Li, Y. Ren, Y. Wang, J. Wu, J. Jia, *Dye. Pigment.* **2022**, *205*, 110572.
[41] Y. Wang, Y. Yang, C. Wei, P. Yu, X. Cheng, J. Li, J. Zhao, J. Lin, L. Xie, *Cryst. Growth Des.* **2023**, *23*, 5651–5657.
[42] Q. Di, J. Li, Z. Zhang, X. Yu, B. Tang, H. Zhang, H. Zhang, *Chem. Sci.* **2021**, *12*, 15423–15428.
[43] K. Huang, L. Song, K. Liu, A. Lv, M. Singh, K. Shen, J. Shen, J. Wang, H. Wang, H. Shi, H. Ma, M. Gu, G. Sun, W. Yao, Z. An, W. Huang, *npj Flex. Electron.* **2021**, *5*, 21.
[44] B. Jovanić, B. Radenković, M. Despotović-Zrakić, Z. Bogdanović, D. Barać, *Optik (Stuttg).* **2021**, *226*, 165928.
[45] M. Tian, Y. Gao, P. Zhou, K. Chi, Y. Zhang, B. Liu, *Phys. Chem. Chem. Phys.* **2021**, *23*, 20567–20573.
[46] B. S. Ma, X. D. Wang, F. H. Su, Z. L. Fang, K. Ding, Z. C. Niu, G. H. Li, *J. Appl. Phys.* **2004**, *95*, 933–938.
[47] B. Li, W. Liu, X. Zhu, S. Lin, Y. Yang, Q. Yang, P. Jin, *Phys. Lett. A* **2019**, *383*, 1483–1486.
[48] Y. Liu, Q. Zeng, B. Zou, Y. Liu, B. Xu, W. Tian, *Angew. Chemie Int. Ed.* **2018**, *57*, 15670–15674.
[49] Y. Gu, K. Wang, Y. Dai, G. Xiao, Y. Ma, Y. Qiao, B. Zou, *J. Phys. Chem. Lett.* **2017**, *8*, 4191–4196.
[50] H. Yuan, K. Wang, K. Yang, B. Liu, B. Zou, *J. Phys. Chem. Lett.* **2014**, *5*, 2968–2973.
[51] J. Guan, C. Zhang, D. Gao, X. Tang, X. Dong, X. Lin, Y. Wang, X. Wang, L. Wang, H. H. Lee, J. Xu, H. Zheng, K. Li, H. Mao, *Mater. Chem. Front.* **2019**, *3*, 1510–1517.
[52] A. Makal, J. Krzeszczakowska, R. Gajda, *Molecules* **2019**, *24*.
[53] S. Ghosh, M. K. Mishra, S. B. Kadambi, U. Ramamurty, G. R. Desiraju, *Angew. Chemie Int. Ed.* **2015**, *54*, 2674–2678.
[54] S. Ghosh, M. K. Mishra, S. Ganguly, G. R. Desiraju, *J. Am. Chem. Soc.* **2015**, *137*, 9912–9921.
[55] M. Woińska, S. Grabowsky, P. M. Dominiak, K. Woźniak, D. Jayatilaka, *Sci. Adv.* **2016**, *2*, e1600192.

**TOC GRAPHIC:**

## Mechanical Tuning of Fluorescence Lifetime and Bandgap in an Elastically Flexible Molecular Semiconductor Crystal

Arif Hassan Dar[#,a] Atiqur Rahman[#,a] Srijan Mondal,[a] Argha Barman,[a] Monika Gupta,[a] Pramit K. Chowdhury,[a] and Sajesh P. Thomas*[a]

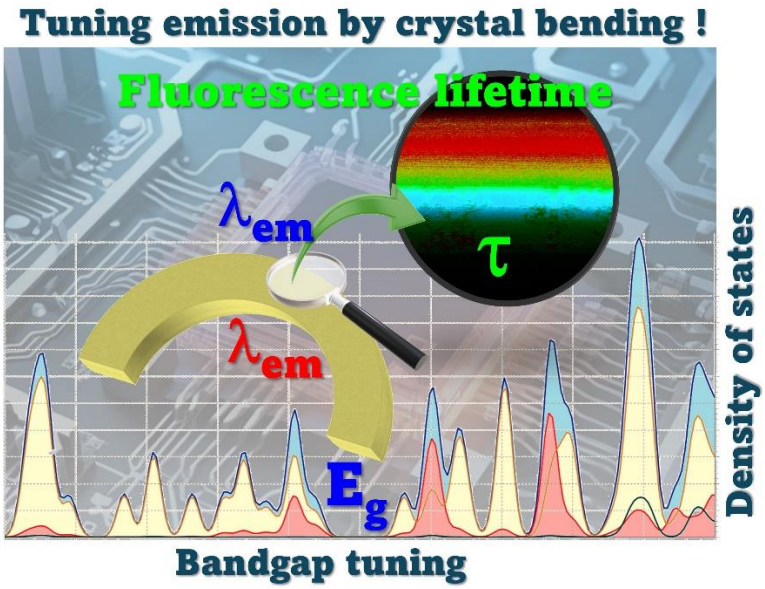


**Bend it to tune it!** Elastic bending of a molecular semiconductor crystal leads to systematic tuning of its electronic bandgap, fluorescence emission wavelengths and a significant variation in lifetime, revealed by our spatially resolved study.